Research Article | Vol. 26, No. 2 | 22 Jan 2018 | OPTICS EXPRESS 1997
Optics EXPRESS

Orbital angular momentum-enhanced measurement of rotation vibration using a Sagnac interferometer

Shixiong Xiao,[1] Lidan Zhang,[1] Dan Wei,[1] Fang Liu,[1] Yong Zhang,[1,*] AND Min Xiao[1,2]

[1]*National Laboratory of Solid State Microstructures, College of Engineering and Applied Sciences and School of Physics, Nanjing University, Nanjing 210093, China*
[2]*Department of Physics, University of Arkansas, Fayetteville, Arkansas 72701, USA*
[*]*zhangyong@nju.edu.cn*

Abstract: We construct an experimental measurement system for rotation vibration signal detection using the orbital angular momentum (OAM) of light in a Sagnac interferometer. Inputting light beams with different OAM, we demonstrate that the measured signal and signal-to-noise ratio can be increased by the OAM mode index *l*. In addition, the Sagnac interferometer can further improve the vibration signal and suppress the environmental noises. Such system has potential applications in high-precision sensing and monitoring of rotation vibrations.

OCIS codes: (270.5290) Photon statistics; (350.5730) Resolution; (120.3180) Interferometry.

References and links

1. L. Allen, M. W. Beijersbergen, R. J. C. Spreeuw, and J. P. Woerdman, "Orbital angular momentum of light and the transformation of Laguerre-Gaussian laser modes," Phys. Rev. A **45**(11), 8185–8189 (1992).
2. P. Genevet, J. Lin, M. A. Kats, and F. Capasso, "Holographic detection of the orbital angular momentum of light with plasmonic photodiodes," Nat. Commun. **3**, 1278 (2012).
3. M. W. Beijersbergen, L. Allen, H. E. L. O. van der Veen, and J. P. Woerdman, "Astigmatic laser mode converters and transfer of orbital angular momentum," Opt. Commun. **96**(1-3), 123–132 (1993).
4. K. Sueda, G. Miyaji, N. Miyanaga, and M. Nakatsuka, "Laguerre-Gaussian beam generated with a multilevel spiral phase plate for high intensity laser pulses," Opt. Express **12**(15), 3548–3553 (2004).
5. L. Marrucci, C. Manzo, and D. Paparo, "Optical Spin-to-Orbital Angular Momentum Conversion in Inhomogeneous Anisotropic Media," Phys. Rev. Lett. **96**(16), 163905 (2006).
6. N. Matsumoto, T. Ando, T. Inoue, Y. Ohtake, N. Fukuchi, and T. Hara, "Generation of high-quality higher-order Laguerre-Gaussian beams using liquid-crystal-on-silicon spatial light modulators," J. Opt. Soc. Am. A **25**(7), 1642–1651 (2008).
7. R. Zheng, C. Gu, A. Wang, L. Xu, and H. Ming, "An all-fiber laser generating cylindrical vector beam," Opt. Express **18**(10), 10834–10838 (2010).
8. N. Passilly, R. de Saint Denis, K. Aït-Ameur, F. Treussart, R. Hierle, and J.-F. Roch, "Simple interferometric technique for generation of a radially polarized light beam," J. Opt. Soc. Am. A **22**(5), 984–991 (2005).
9. D. Wei, J. Guo, X. Fang, D. Wei, R. Ni, P. Chen, X. Hu, Y. Zhang, W. Hu, Y. Q. Lu, S. N. Zhu, and M. Xiao, "Multiple generations of high-order orbital angular momentum modes through cascaded third-harmonic generation in a 2D nonlinear photonic crystal," Opt. Express **25**(10), 11556–11563 (2017).
10. D. Wei, Y. Zhu, W. Zhong, G. Cui, H. Wang, Y. He, Y. Zhang, Y. Lu, and M. Xiao, "Directly generating orbital angular momentum in second-harmonic waves with a spirally-poled nonlinear photonic crystal," Appl. Phys. Lett. **110**(26), 261104 (2017).
11. G. Gibson, J. Courtial, M. Padgett, M. Vasnetsov, V. Pas'ko, S. Barnett, and S. Franke-Arnold, "Free-space information transfer using light beams carrying orbital angular momentum," Opt. Express **12**(22), 5448–5456 (2004).
12. Y. Yan, G. Xie, M. P. J. Lavery, H. Huang, N. Ahmed, C. Bao, Y. Ren, Y. Cao, L. Li, Z. Zhao, A. F. Molisch, M. Tur, M. J. Padgett, and A. E. Willner, "High-capacity millimetre-wave communications with orbital angular momentum multiplexing," Nat. Commun. **5**, 4876 (2014).
13. Y. Ren, L. Li, Z. Wang, S. M. Kamali, E. Arbabi, A. Arbabi, Z. Zhao, G. Xie, Y. Cao, N. Ahmed, Y. Yan, C. Liu, A. J. Willner, S. Ashrafi, M. Tur, A. Faraon, and A. E. Willner, "Orbital angular momentum-based space division multiplexing for high-capacity underwater optical communications," arXiv:1604.06865 (2016).
14. M. F. Andersen, C. Ryu, P. Cladé, V. Natarajan, A. Vaziri, K. Helmerson, and W. D. Phillips, "Quantized rotation of atoms from photons with orbital angular momentum," Phys. Rev. Lett. **97**(17), 170406 (2006).

#315023 https://doi.org/10.1364/OE.26.001997
Journal © 2018 Received 5 Dec 2017; revised 13 Jan 2018; accepted 14 Jan 2018; published 18 Jan 2018

Optics EXPRESS

15. H. Bechmann-Pasquinucci and A. Peres, "Quantum Cryptography with 3-State Systems," Phys. Rev. Lett. **85**(15), 3313–3316 (2000).
16. H. Bechmann-Pasquinucci and W. Tittel, "Quantum cryptography using larger alphabets," Phys. Rev. A **61**(6), 062308 (2000).
17. L. Zhang, C. Silberhorn, and I. A. Walmsley, "Secure quantum key distribution using continuous variables of single photons," Phys. Rev. Lett. **100**(11), 110504 (2008).
18. S. P. Walborn, D. S. Lemelle, M. P. Almeida, and P. H. S. Ribeiro, "Quantum key distribution with higher-order alphabets using spatially encoded qudits," Phys. Rev. Lett. **96**(9), 090501 (2006).
19. P. B. Dixon, G. A. Howland, J. Schneeloch, and J. C. Howell, "Quantum mutual information capacity for high-dimensional entangled states," Phys. Rev. Lett. **108**(14), 143603 (2012).
20. M. P. Lavery, F. C. Speirits, S. M. Barnett, and M. J. Padgett, "Detection of a spinning object using light's orbital angular momentum," Science **341**(6145), 537–540 (2013).
21. M. Zhao, X. Gao, M. Xie, W. Zhai, W. Xu, S. Huang, and W. Gu, "Measurement of the rotational Doppler frequency shift of a spinning object using a radio frequency orbital angular momentum beam," Opt. Lett. **41**(11), 2549–2552 (2016).
22. H. Zhou, D. Fu, J. Dong, P. Zhang, and X. Zhang, "Theoretical analysis and experimental verification on optical rotational Doppler effect," Opt. Express **24**(9), 10050–10056 (2016).
23. G. Li, T. Zentgraf, and S. Zhang, "Rotational Doppler effect in nonlinear optics," Nat. Phys. **12**(8), 736–740 (2016).
24. Z. Zhang, T. Qiao, K. Ma, L. Cen, J. Zhang, F. Wang, and Y. Zhao, "Ultra-sensitive and super-resolving angular rotation measurement based on photon orbital angular momentum using parity measurement," Opt. Lett. **41**(16), 3856–3859 (2016).
25. E. Distante, M. Ježek, and U. L. Andersen, "Deterministic Superresolution with Coherent States at the Shot Noise Limit," Phys. Rev. Lett. **111**(3), 033603 (2013).
26. X. M. Feng, G. R. Jin, and W. Yang, "Quantum interferometry with binary-outcome measurements in the presence of phase diffusion," Phys. Rev. A **90**(1), 013807 (2014).
27. Z. Zhang, T. Qiao, K. Ma, J. Zhang, L. Cen, F. Wang, and Y. Zhao, "Super-resolving angular rotation measurement using binary-outcome homodyne detection," Opt. Express **24**(16), 18477–18484 (2016).
28. J. J. Bollinger, W. M. Itano, D. J. Wineland, and D. J. Heinzen, "Optimal frequency measurements with maximally correlated states," Phys. Rev. A **54**(6), R4649–R4652 (1996).
29. C. C. Gerry, A. Benmoussa, and R. A. Campos, "Nonlinear interferometer as a resource for maximally entangled photonic states: Application to interferometry," Phys. Rev. A **66**(1), 013804 (2002).
30. C. C. Gerry and J. Mimih, "The parity operator in quantum optical metrology," Contemp. Phys. **51**(6), 497–511 (2010).
31. L. Cohen, D. Istrati, L. Dovrat, and H. S. Eisenberg, "Super-resolved phase measurements at the shot noise limit by parity measurement," Opt. Express **22**(10), 11945–11953 (2014).
32. S. Slussarenko, V. D'Ambrosio, B. Piccirillo, L. Marrucci, and E. Santamato, "The polarizing Sagnac interferometer: a tool for light orbital angular momentum sorting and spin-orbit photon processing," Opt. Express **18**(26), 27205–27216 (2010).
33. F.-X. Wang, W. Chen, Y.-P. Li, G.-W. Zhang, Z.-Q. Yin, S. Wang, G.-C. Guo, and Z.-F. Han, "Single-path Sagnac interferometer with Dove prism for orbital-angular-momentum photon manipulation," Opt. Express **25**(21), 24946–24959 (2017).
34. O. S. Magaña-Loaiza, M. Mirhosseini, B. Rodenburg, and R. W. Boyd, "Amplification of Angular Rotations Using Weak Measurements," Phys. Rev. Lett. **112**(20), 200401 (2014).
35. F. I. Moxley III, J. P. Dowling, W. Dai, and T. Byrnes, "Sagnac interferometry with coherent vortex superposition states in exciton-polariton condensates," Phys. Rev. A **93**(5), 053603 (2016).
36. N. González, G. Molina-Terriza, and J. P. Torres, "How a Dove prism transforms the orbital angular momentum of a light beam," Opt. Express **14**(20), 9093–9102 (2006).
37. M. O. Scully and J. P. Dowling, "Quantum-noise limits to matter-wave interferometry," Phys. Rev. A **48**(4), 3186–3190 (1993).
38. A. K. Jha, G. S. Agarwal, and R. W. Boyd, "Supersensitive measurement of angular displacements using entangled photons," Phys. Rev. A **83**(5), 053829 (2011).
39. S. Li, Q. Mo, X. Hu, C. Du, and J. Wang, "Controllable all-fiber orbital angular momentum mode converter," Opt. Lett. **40**(18), 4376–4379 (2015).
40. F. Liu, Y. Zhou, J. Yu, J. Guo, Y. Wu, S. Xiao, D. Wei, Y. Zhang, X. Jia, and M. Xiao, "Squeezing-enhanced fiber Mach-Zehnder interferometer for low-frequency phase measurement," Appl. Phys. Lett. **110**(2), 021106 (2017).

1. Introduction

It has been approximately 25 years since the first research was undertaken on the orbital angular momentum (OAM) of light [1]. One major research direction is the development of OAM generation methods, with earlier methods, including use of forked holograms [2], astigmatic mode converters [3] and other devices [4–6], being augmented by newer methods

Optics EXPRESS

based on optical fibers [7], interferometric methods [8] and nonlinear optical techniques [9, 10]. Apart from the technical innovation and improvement of OAM generation, applications of OAM are also hot research topics. One remarkable characteristic of OAM is its orthogonality. Using classical coherent states, the OAM of light can be applied in communications [11–13] to achieve high capacity, and micromanipulation [14] can also be performed via OAM. When combined with quantum characteristics, OAM light beams with different values of mode index l can produce high-dimensional entanglement to provide increased security and robustness [15–17] and high information capacities [16–19] for quantum communications.

Another interesting characteristic is its vortex wavefront, which enables use of the OAM of light in rotation measurements [20–23]. Generally, the reported methods utilize the geometric phase distribution of the OAM light to perform static weak rotation angle measurements with low photon numbers [24]. A Mach-Zehnder interferometer is normally used in the measurement. Under these conditions, there are several ways to measure the weak rotation angle: the binary outcome homodyne detection (BHD) method [25–27], the parity detection (PD) method [28–30], and the Z detection (ZD) method [31]. There are also many works using Sagnac interferometer to manipulate OAM light for sorting [32, 33], weak measurement [34] and exciton-polariton condensates [35]. However, these methods are limited in static measurements. In practical applications, dynamic rotation vibration measurements are more commonly required, which can also be detected and amplified by use of OAM.

Our experiment uses the geometric phase distribution of the OAM to amplify the rotation signal by the mode index l of the OAM. We use a Sagnac interferometer rather than a Mach-Zehnder interferometer to double the signal amplitude. In the experiment, we demonstrate the OAM-enhanced measurement of low single-frequency vibration signals while simultaneously reducing the environmental noise. The above advantages make this measurement method more practical.

2. Theory

Consider the situation where two coherent lights with OAM of l pass through a Sagnac interferometer. A Sagnac interferometer can be considered as a Mach-Zehnder interferometer in which the two arms share one light path. As shown in Fig. 1, the two arms pass through a Dove prism oriented at an angle of θ. Dove prism is an optical element that can rotate a light beam by $\pi - 2l\theta$, where l is the OAM mode index of the beam and θ is the rotation angle of the prism [36]. Mathematically, the Dove prism can cause a phase change of $\pi - 2l\theta$ in an OAM light beam that passes through it. If the Dove prism vibrates within a small angle θ, a measurable signal will be produced. Next, we calculate the signal-to-noise ratio (SNR) under such experimental configuration.

Optics EXPRESS

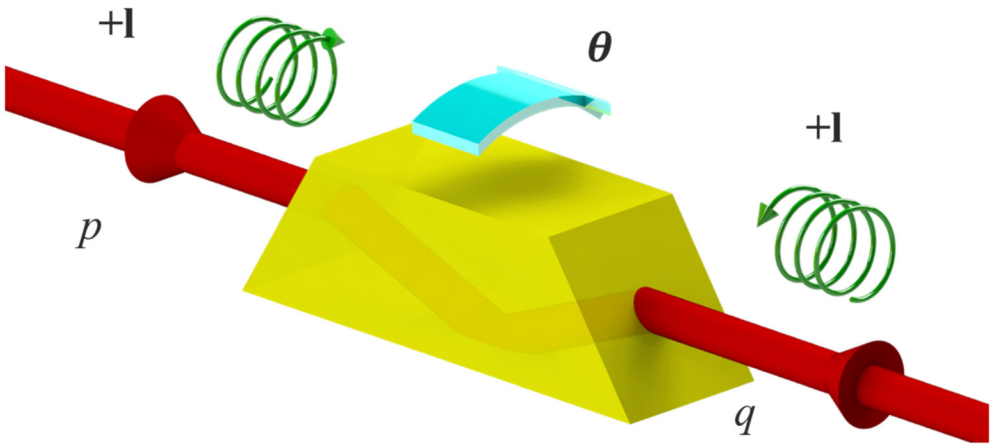

Fig. 1. Illustration of an OAM beam passing through a Dove prism. Two light beams (p and q) with the same l pass through the Dove prism in opposite directions. The Dove prism gives the two light beams opposite phase changes.

Assuming that two input modes are a and b, the two outputs a_{out} and b_{out} are

$$\begin{pmatrix} a_{out} \\ b_{out} \end{pmatrix} = \frac{1}{2}\begin{pmatrix} 1 & 1 \\ 1 & -1 \end{pmatrix}\begin{pmatrix} e^{i\varphi} & 0 \\ 0 & e^{-i\varphi} \end{pmatrix}\begin{pmatrix} 1 & 1 \\ 1 & -1 \end{pmatrix}\begin{pmatrix} a \\ b \end{pmatrix}. \tag{1}$$

Here, φ is the phase difference between two arms. Since b is vacuum state under our experimental configuration, the intensity measurements of two detectors $I_{a_{out}}$ and $I_{b_{out}}$ are

$$\begin{aligned} I_{a_{out}} &= \cos^2\varphi\left\langle a^{\dagger}a\right\rangle = |\alpha|^2\cos^2\varphi, \\ I_{b_{out}} &= \cos^2\varphi\left\langle a^{\dagger}a\right\rangle = |\alpha|^2\sin^2\varphi \end{aligned} \tag{2}$$

where α is the complex amplitude of the light. The intensity difference I^- is

$$I^- = |I_a - I_b| = |\alpha|^2\cos 2\varphi. \tag{3}$$

In Eq. (3), $\varphi \propto 2l\theta$ with θ being the rotation angle of dove prism. When the Sagnac interferometer is locked at $\pi/2$ and θ is sufficiently small, the signal and the signal-to-noise ratio satisfy [37, 38]

$$\partial I^-/\partial\theta \propto 4l|\alpha|^2, \tag{4}$$

$$SNR \propto \frac{|\partial I^-/\partial\theta|}{|\Delta I^-|} \propto l|\alpha|^2. \tag{5}$$

Because our system works in the low frequency band, the classical noise dominates ΔI^-, which does not change significantly with different OAM of light as demonstrated in our experiment. Then, we can get $SNR \propto l$.

Unlike the Mach-Zehnder interferometer case, the OAM light beams in the two arms of the Sagnac interferometer pass through the Dove prism in opposite directions. As a result, the signal will be doubled while the noise will remain unchanged in comparison to the Mach-Zehnder interferometer case.

Optics EXPRESS

3. Experimental Configuration

The laser used was an ultra-narrow linewidth continuous wave diode-pumped solid-state laser (Coherent Co.) operating at 1064 nm. The output laser was focused onto a forked grating to generate the OAM. To determine how the signal changed along with the index l, we placed ten different forked gratings with mode indices ranging from $l = 1$ to 10 on a single plate to allow the OAM to be changed easily. The subsequent half-wave plate was used to adjust the polarization (Fig. 2).

We first launched the light with OAM into a Mach-Zehnder interferometer for two reasons. First, this allowed us to sweep the Sagnac interferometer. Because the two arms share the same path in the Sagnac interferometer and the two light beams are reflected by the same mirrors, it is difficult to sweep the interferometer. In our experiment, the input polarization is first rotated to 45° by a half-wave plate (HWP). In the Mach-Zehnder interferometer, the input light is divided into *a* and *b* modes by PBS1, which have horizontal and vertical polarizations, respectively. Then, they combine at PBS2 and enter the Sagnac interferometer. By using PBS3, the *c* and *d* modes in the Sagnac interferometer have orthogonal polarizations. Under such configuration, the relative phase between *c* and *d* modes in the Sagnac interferometer is equivalent to that between *a* and *b* modes in the Mach-Zehnder interferometer. By setting a piezoelectric transducer (PZT) in the Mach-Zehnder interferometer, we can sweep the Sagnac interferometer. Second, this allowed us to lock the Sagnac interferometer phase on $\pi/2$. The signal normally shows a small variance. Under specific circumstances, we lock the Sagnac interferometer on a phase of $\pi/2$, which provides the highest slope to produce the best possible signal we want to measure. When locked, the PZT controls one mirror in the Mach-Zehnder interferometer to maintain the phase difference in the Sagnac interferometer using the signal produced by a Proportion Integration Differentiation (PID).

Here, we obtain the error signal by a beam splitter (BS) before the Sagnac interferometer, which means the environmental noise in Mach-Zehnder interferometer can be compensated but the signal to measure in Sagnac interferometer will not be affected. However, it may cause another problem that the environmental noise in Sagnac interferometer cannot be compensated. Fortunately, in the Sagnac interferometer, the two light beams share the same path after the BS, which means that even if turbulence occurs, the two light beams will be affected in the same way. Therefore, the interferometer system can remain stable under our locking method.

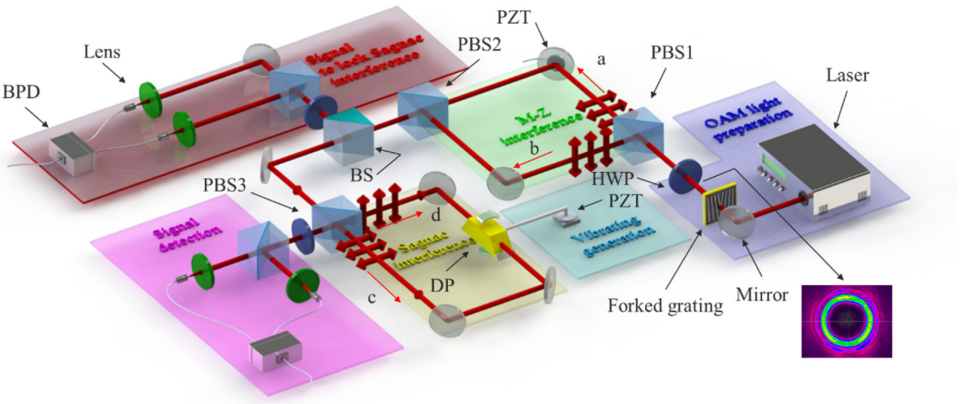

Fig. 2. Experimental setup. There are six sections: (1) OAM light generation; (2) Mach-Zehnder interferometer; (3) Signal locking; (4) Sagnac interferometer; (5) Vibration generation; (6) Signal detection. HWP: half-wave plate, PBS: polarization beam splitter; BPD: balanced photodetectors; BS: beam splitter; DP: Dove prism; PZT: piezoelectric transducer.

Optics EXPRESS

The core of the system is the Sagnac interferometer. The number of mirrors in the Sagnac interferometer must be considered because the sign of the mode index of the OAM light will be reversed after a single reflection. According to the theory, there must be two OAM light beams with the same index passing through the Dove prism in opposite directions. In the first PBS, one light beam is reflected while the other is not, which means that there should be an odd number of mirrors after the PBS. The lowest number that can be used is three mirrors, which can be used along with one PBS to construct a square loop. In this loop, the Dove prism can be placed between any two of the mirrors.

4. Results

4.1. Static measurements

According to the theory above, when the Dove prism is continuously rotated to different angles, the output light power will be modulated periodically. From Eq. (3), we can see that the period T is dependent on the mode index l of the OAM beam, i.e., $T = 2\pi/(2\times 2\times l) = \pi/2l$. Figure 3 shows the measured results with an input l = 5, from which we can calculate the period T = 18 degree.

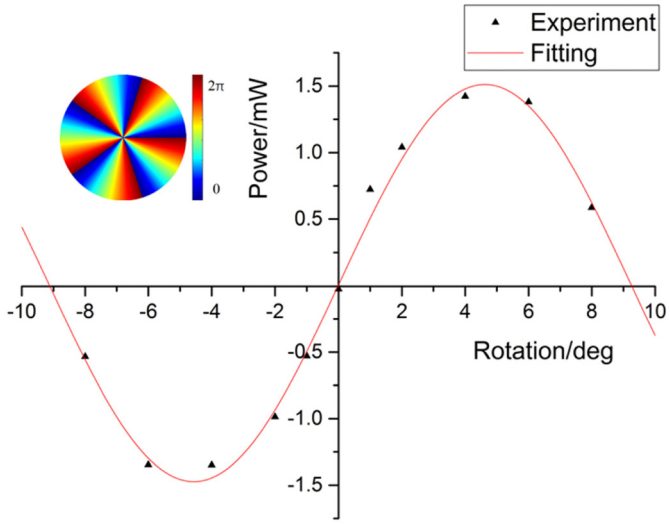

Fig. 3. Sweep of the rotation angle of the Dove prism. The black points are measured from the Sagnac interferometer with l = 5 and the red line is a fitting curve. Inset shows the phase distribution of the OAM mode l = 5.

Optics EXPRESS

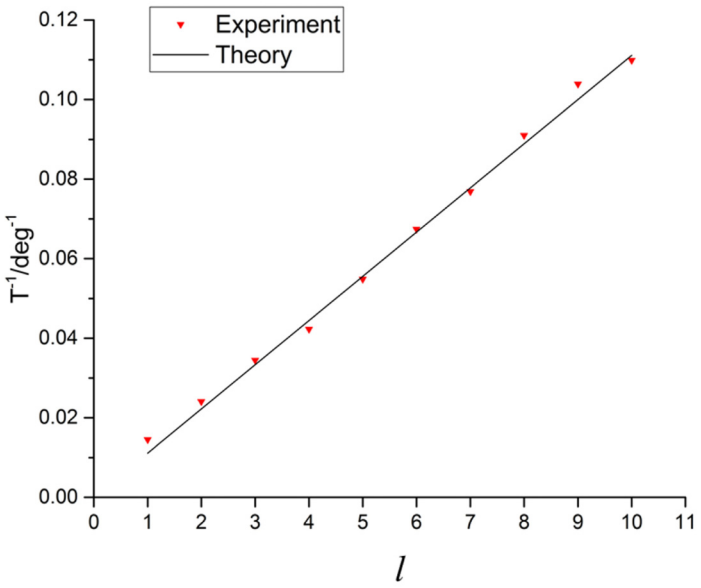

Fig. 4. Measurement of a static rotation angle using different OAM light beams with indices ranging from $l = 1$ to 10.

Figure 4 shows the dependence of T on the input l. We used the method shown in Fig. 3 to measure the period T for l ranging from 1 to 10. The rotation angle is set to be –90 to 90 degrees. A comparison between the experimental data and the theoretical calculation results is given. The black line indicates the theoretical calculation results and the red points were calculated from the experimental data. Clearly, T is inversely proportional to l as expected. Since T decides the slope in Fig. 3, it is expected that higher l produces higher output power for certain small rotation angle.

4.2. Vibration frequency measurement and signal amplitude

Vibration frequency measurements require the analysis of the frequency spectrum of the signal. Because the operating frequency range here is from 300 Hz to 800 Hz, we use a fast Fourier transform (FFT) for the analysis. The range of the FFT is from 100 Hz to 1.1 kHz, and the frequency resolution is 0.1 Hz. According to the FFT, if A and A' represent the amplitudes before and after the FFT, respectively, then we will have

$$A' = NA/2, \tag{6}$$

where N is the number of samples. First, we measured the frequency response of the vibration system (including PZT, dove prism and the connection components). Under input power of 2 mW and using OAM light with $l = 10$, three peaks occur at 320 Hz, 430 Hz and 650 Hz that represent the highest responses of the system. We then selected these three peaks to carry out the experiment.

Optics EXPRESS

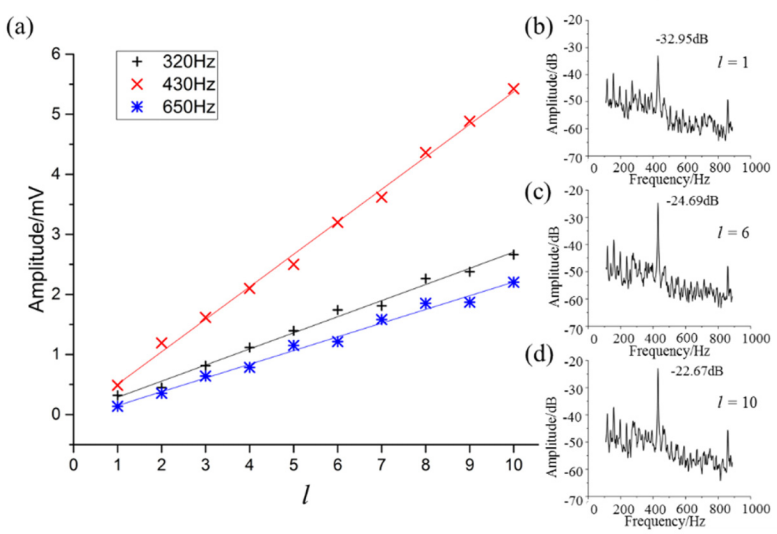

Fig. 5. (a) Vibration signal amplitude versus *l*. Because the frequency response of the system, the measured results at different frequencies have different slopes. (b)-(d) show the measured results with a vibration signal at 430 Hz, which are −32.95dB (0.51mV) at l = 1, −24.69dB (3.40mV) at l = 6 and −22.67dB (5.41mV) at l = 10.

Figure 5 shows the dependence of the measured amplitude of the vibration signal on the input *l*. Similarly to the static measurement results, when the maximal vibration angle remains stable, higher *l* produces higher amplitude in the measurement. Because the vibration angle θ is sufficiently small (θ = 1~2 degree) in the experiment, Eq. (4) indicates that the measured signal can be considered to be linearly dependent on *l*. We can see from Fig. 5(a) that, under an input light power of 1 mW, the signal amplitude is basically linearly dependent on *l*. It should be noted that the three lines in Fig. 5(a) have different slopes, which may be attributed to that the vibration system has different responses at different frequencies. Therefore, one should carefully choose the optical components to achieve good response for the vibration frequency to be measured.

Optics EXPRESS

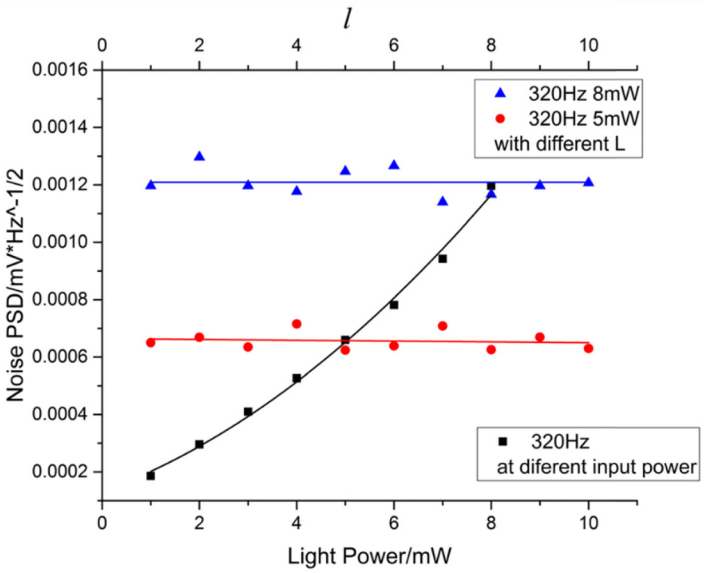

Fig. 6. System noises with different OAM light beams. When the signal is 320 Hz and the OAM mode index is $l = 10$, the black line shows the system noise at different input power. The blue line and the red line show the noise features of the different OAM light beams with 8mW and 5mW input power, respectively.

We have proved that the vibration signal can be amplified using the OAM of light in a Sagnac interferometer. Next, we analyze the noise of the vibration measurement system. In Fig. 6, we can see the system is not completely shot-noise-limited because the black line shows a squared rather than linear relationship. It should be noted that it is very hard to reach the shot noise limit in the low frequency band. When the input power was maintained at 5 mW and 8 mW, we measured the noises for different OAM light beams. One can see that the noise is basically irrelevant to the OAM mode in Fig. 6. Considering that the signal is enhanced by OAM of light and the Sagnac interferometer, the SNR under our experimental configuration is improved by a factor of $2l$. Since our system still does not reach the shot noise limit, the SNR can be further improved by suppressing the classical noises of the system.

5. Conclusion

In summary, we have demonstrated a system that can be used to measure vibration signals. The system SNR is amplified by using OAM. In addition, use of a Sagnac interferometer allowed us to double the signal without changing the noise in comparison to the Mach-Zehnder case. Further improvements can be made to the proposed system. For example, optical fiber interferometer [39] can make the system more convenient and portable. Second, the system can be combined with squeezed light, which will give the system the ability to perform high-precision measurements beyond the shot noise limit [40].

Funding

National Key R&D Program of China (2017YFA0303700, 2016YFA0302500); National Natural Science Foundation of China (NSFC) (91636106, 11621091, 61605072); Nanjing University Innovation and Creative Program for PhD candidate (CXCY17-27); Postgraduate Research & Practice Innovation Program of Jiangsu Province (KYCX17_0028).